This is a peer-reviewed, accepted author manuscript of the following research article:
Fan, F., Nwobu, J., & Campos-Gaona, D. (Accepted/In press). Co-located battery energy storage optimisation for dynamic containment under the UK frequency response market reforms. CSEE Journal of Power and Energy Systems, 1-12. https://doi.org/10.17775/CSEEJPES.2023.01210

Co-located Battery Energy Storage Optimisation for Dynamic Containment under the UK Frequency Response Market Reforms

Fulin Fan, John Nwobu, and David Campos-Gaona, *Senior Member*, *IEEE*

***Abstract*—The accelerated development of battery technologies heightens an interest in co-locating battery energy storage systems (BESSs) with renewable power plants for the stacking of multiple revenue streams such as frequency response services to AC grids. The frequency response market reforms in the UK introduce new end-state services and require evaluating the techno-economic feasibility of co-location projects in new circumstances. This paper develops a BESS optimisation method to optimise the capacity and operating strategy of a co-located BESS for providing the latest Dynamic Containment (DC) services based on the UK perspective. The BESS optimisation method simulates the BESS delivering DC responses and following operational baselines for state of energy (SoE) restoration as well as coordinating with its co-located power plant. Then the net present value of the BESS co-location project is estimated from power flows across the system and maximised to suggest the optimal BESS capacity, target energy footroom and/or headroom levels for baseline estimation, and possible SoE ranges suitable for energy interchange with its co-located power plant. The BESS optimisation method is tested based on a particular transmission-level wind farm in the UK and discussed alongside the operation and profitability of a BESS co-location project under frequency response market reforms.**

***Index Terms*—Battery energy storage optimisation, co-location, Dynamic Containment, operating strategy, UK perspective**

NOMENCLATURE

t, Δt	Time step index and length.
i	Settlement period (SP) index.
e	Electricity Forward Agreement (EFA) index.
k	Cycle index.
d	Day index.
m	Month index.
DC	Dynamic Containment.
P_{DC}^{LF}, P_{DC}^{HF}	Contracted low-frequency (LF) or high-frequency (HF) DC power capacity.
MER	Minimum Energy Requirement for DC.
WF	Wind Farm.
P_{WF}^{tot}	Available wind power output.
P_{WF}^{sell}	Wind power sold to AC grid across WF meter.
P_{WF}^{str}	Wind power transferred to battery side.
P_{WF}^{cur}	Wind power curtailment.
P_C	Connection point ampacity.
BESS	Battery Energy Storage System.
AdC	Additional Converter between WF and BESS.
P_B^R, P_A^R	Rated power capacity of BESS or AdC.
η	Power conversion efficiency.
c	Half or full cycle indicator.
soc	State of charge (SoC).
dod	Depth of discharge (DoD).
t_E	Elapsed time period.
T_c	Cell temperature.
$f(\cdot)$	Battery degradation function.
$S(\cdot)$	Battery stress model.
γ	Stress model coefficients.
λ, β	Energy capacity fading coefficients.
E_B^R, $\overline{E}_B$	Rated or remaining energy capacity of BESS.
E_i^t	State of energy (SoE) at time step t in SP i.
E_{ft}	Target initial energy footroom for LF DC.
E_{hd}	Target initial energy headroom for HF DC.
P_B^{op}	Power output of BESS across DC meter.
P_B^{DC}	DC response of BESS.
P_B^{BL}	Operational baseline of BESS.
P_B^{sell}	BESS export to WF meter via AdC.
α_{ch}	Variable specifying SoE limit E_{ch} on P_{WF}^{str}.
α_{dis}	Variable specifying SoE limit E_{dis} on P_B^{sell}.
σ	Minimum SoC limit.
NPV	Net present value.
R, C, δ	Revenue, cost, or its change after co-location.
$\mathcal{P}$	Unit price in £/MWh or £/MW/h.

I. INTRODUCTION

BATTERY energy storage systems (BESSs) are increasingly viewed as a key component permitting the delivery of low carbon, more flexible and more decentralised energy [1]. With the fast growth of battery markets and the rapid development of battery technologies in recent years [2], it expects to see an increase in the co-location of BESSs with existing power plants [3]. This is in particular an attractive option for renewable power plants where the co-located BESSs not only manage the intermittent nature of renewable generation [4] but can also supply ancillary services to the main grids [5] using the existing connection point and infrastructure.

From a number of ancillary services in the UK [6], frequency response (FR) services are the suitable products to BESSs that

F. Fan, and D. Campos-Gaona are with the Department of Electronic and Electrical Engineering, University of Strathclyde, Glasgow, G1 1XW, U.K. (e-mail: f.fan@strath.ac.uk; d.campos-gaona@strath.ac.uk).

J. Nwobu is with the Offshore Renewable Energy Catapult, Glasgow, G1 1RD, U.K. (e-mail: john.nwobu@ore.catapult.org.uk).

can respond to grid frequency deviations or instructions issued by the National Grid Electricity System Operator (NGESO) within a sub-second time-frame [7]. The NGESO procures FR services either through the mandatory FR offered by particular transmission-connected generators [6] or through commercial arrangements such as Firm FR (FFR) auctioned on a monthly basis [8] and Enhanced FR (EFR) contracted for four years [9]. As the UK transitions to a low-carbon economy, the FR markets not only require the development of new fast-acting products to counterbalance the system inertia reduction [10] but also see an increased diversity in the FR provider base [11]. To permit the carbon-free electricity system operation by 2025, the NGESO is reforming the FR markets to make products more accessible for all technologies by procuring FR services closer to real-time, standardising their requirements and replacing the existing FR products with a new integrated suite of services [11]. A weekly FR auction trial was launched in November 2019 to test closer-to-real-time procurement of FR services [11] with the release of interim services including Dynamic Low High (DLH) which standardises the FFR with equal capacities of low and high FR [12]. The Dynamic Containment (DC), i.e., one of the new end-state services, was introduced in October 2020 to meet the need for faster-acting post-fault FR that is designed for a significant frequency deviation [13]. In addition, to lower the barriers to the DC market entry for energy-limited assets like BESSs, the NGESO allows BESSs to manage state of energy (SoE) levels by constantly submitting and following operational baselines in each 30-min settlement period (SP). The NGESO also specifies the SoE Rules to indicate the minimum energy footroom and/or headroom that BESSs must start with over a contracted service window and the minimum energy that BESSs must restore via baselines in a SP. The compliance with the SoE Rules allows BESSs to enter the DC market and avoid penalties for any DC under-delivery [14]. The introduction of DC and other end-state services requires evaluating the techno-economic feasibility of BESS co-location projects in new circumstances, which largely depends on the optimisation of the BESS size and operation.

Most research related to the economic optimisation of stand-alone or co-located BESSs for frequency regulation or FR deals with a trade-off in the BESS size and/or operating strategies between the BESS investment and the FR service performance. The tendering and operating strategies of a stand-alone BESS in the UK FFR market or the US PJM regulation market were optimised in [15] or [16] respectively, which suggested the time duration for battery energy management and the minimum FFR tendered prices [15] or the highest FR capacity to be bid while ensuring the required FR delivery performance [16]. The effects of BESS cycles on battery lifetime reductions were additionally taken into account by [17] to optimise the operating and bidding strategies for the BESS that simultaneously participated in the day-ahead energy, frequency regulation and reserve markets. In the cases of the BESS co-located with renewable power plants such as wind farms (WFs), most research has considered using the BESS to deliver FR services to the main grid via the existing connection point or assist the WF in the FR provision. Based on the market mechanisms and historic clearing prices of EFR and DLH services, the optimum sizes and operating strategies of the BESSs co-located with existing WFs for the FR provision were estimated in [5] and [18] respectively; the DLH service capacity and service windows to be tendered for in weekly auctions were additionally optimised in [18] to maximise the net present value (NPV) of the co-location project from which the possible lowest DLH tendered prices were inferred. Furthermore, the savings of connection costs by sharing the existing electrical infrastructure of WFs were identified to be one of the key factors contributing to a profitable BESS project [5]. For the WF which must reserve part of its available power outputs for low-frequency responses (or upward regulation), the BESS operation was optimised in [19] and [20] in order for the WF to export close to its available outputs. Considering that wind power prediction errors would degrade the service performance of a WF, the co-located BESS has also been used to compensate for insufficient and inaccurate wind power outputs [21], [22]. In [23], the WF and the BESS were considered as a whole by combining available wind power outputs with available battery outputs in the bids for day-ahead and FR-related service markets. In addition to FR services and energy markets, some research was also devoted to optimising BESSs for the stacking of other revenue streams such as those from the black start [24] and energy arbitrage [25]-[27].

The contribution of this paper is to fully reflect the market mechanisms and requirements of the UK's latest DC service in the BESS operation, and develop a BESS optimisation method for a transmission-level WF owner to co-optimise the size and operating strategies of its co-located BESS as well as the power capacity contracted for the DC with the objective of the NPV maximisation. Since the SoE Rules require a BESS starting a 4-hr service window with an initial SoE level that can deliver low-frequency (LF) and/or high-frequency (HF) DC responses at the contracted power capacity for at least 15 minutes [14], the operating strategies proposed here specify the target level(s) of initial energy footroom and/or headroom respectively, towards which the SoE level is restored by submitting and following the operational baselines in each 30-min SP. The optimised rise of the target energy footroom/headroom level above the 15-min full-response energy requirement enables a reasonably sized BESS to deal with the uncertainties of grid frequencies that would occur until the end of the 30-min baselines in question, ensuring the fulfilment of the energy requirement at the start of most service windows. Furthermore, the baselines in a 30-min SP are particularly regulated to fully comply with the ramp rate limits specified by the SoE Rules while reducing the gap from the target energy level(s). In addition, the coordination between WF and BESS is designed here to prioritise the DC provision, followed by the time shift of wind generation which is regulated by two additional SoE variables that constrain the BESS export to the WF side and the import of wind curtailment respectively. In order to understand the respective and joint effects of LF and HF DC service provision on the BESS sizing and operation as well as the co-location project's profits, the BESS optimisation method is tested based on a transmission-level WF in the UK when the BESS is co-located to provide either or both LF and HF DC services separately. This provides WF owners with insights into the techno-economics of developing BESS co-location projects under the UK's latest FR market reforms.

The paper is structured as follows: Section II introduces the UK's end-state FR services and designs operating strategies of BESS co-location systems for DC delivery; Section III models expenses and benefits of co-location projects and implements the particle swarm optimisation algorithm; Section IV discusses the optimisation results and the techno-economic performance of co-location projects; and Section V presents conclusions.

II. Operating Strategies of BESS for Dynamic Containment Delivery

A. Dynamic Containment Service

1) Technical requirements

The integrated suite of end-state services being developed in the UK's FR markets comprises Dynamic Containment (DC), Dynamic Moderation, and Dynamic Regulation that deal with different levels of grid frequency deviations from the nominal 50 Hz [10], [11]. The DC is designed to operate post-fault and respond to significant deviations exceeding ±0.2 Hz, as shown in Fig. 1 [13], based on which the required DC response from a provider is determined.

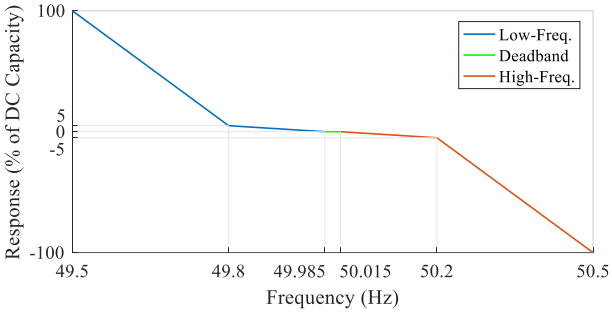

Fig. 1. Frequency response curve for Dynamic Containment (DC) service.

During the soft launch of DC since October 2020, the LF DC is procured day ahead in a service week where participants are allowed to amend prices for the subsequent days [28]. The HF DC is procured separately since November 2021 with the option for participants to link HF bids with LF bids [29]. In addition, a minimum energy requirement (MER) is specified for energy-limited assets which must ensure that their energy capacity can sustain at the full response for at least 15 minutes in either or both directions [13]. To assess the impacts of LF and HF DC on the optimal BESS size and operation, the paper will perform the optimisation for LF-, HF-only or LF+HF DC separately.

2) Operational baseline and SoE Rules [14]

Considering that energy-limited providers like BESSs are not able to continuously deliver DC, BESSs are allowed to manage SoE levels by submitting and following operational baselines in 30-min SPs while providing the DC to AC grids. In addition, the NGESO has particularly designed the SoE Rules indicating that BESSs must start a 4-hr contracted service window (in line with electricity forward agreement (EFA) blocks) with an initial energy footroom or headroom level that meets the MER for the LF or HF DC respectively. Furthermore, the SoE Rules require BESSs restoring at least 20% of the MER in each SP via their operational baselines which must comply with a ramp rate limit equalling 5% of the contracted DC capacity per min. The BESS satisfying the SoE Rules in a contracted EFA block will receive the full DC availability payment even if its exhausted energy footroom/headroom leads to the DC under-delivery; otherwise, a full DC payment deduction is applied to the contracted block.

Since an operational baseline switching between exporting and importing will go through zero, the exporting or importing baseline of a SP is particularly designed here to be symmetric and ramp up to an amplitude of 2.5% of HF or LF DC capacity (denoted by P_{DC}^{HF} or P_{DC}^{LF}) respectively at the 1st and last minutes of the SP. Then the rate of the baseline ramping up to or down from its maximum amplitude is limited to 5% of P_{DC}^{HF} or P_{DC}^{LF} as required. Fig. 2 shows exemplary baselines with two different maximum amplitudes in each direction. The maximum amplitude of the exporting or importing baseline is determined here by the minimum of (a) the level that it can ramp to in half of a SP (i.e., 72.5% of P_{DC}^{HF} or P_{DC}^{LF} in 15 minutes), (b) the rise of discharging or charging power capacity of the BESS above P_{DC}^{LF} or P_{DC}^{HF} respectively, or (c) the level that allows the BESS to restore the energy required in the SP. Given the typical efficiency curves of Li-Ion batteries and converters in Fig. 3(a) [30], the energy that can be restored by a 100 MW BESS in a SP via the baselines of different maximum amplitudes is shown in Fig. 3(b). This will help determine the maximum amplitude and resulting shape of the baselines in a SP given a specific energy restoration requirement, the estimation of which will be detailed in Section II.B.

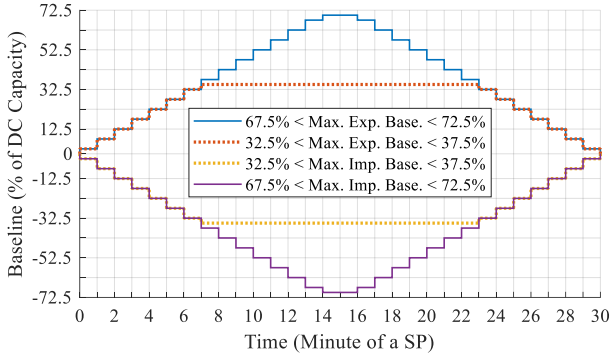

Fig. 2. The ramping of exporting or importing operational baselines (MW) in a SP with the maximum amplitude locating within 67.5% – 72.5% or 32.5% – 37.5% of the contracted HF or LF DC capacity respectively.

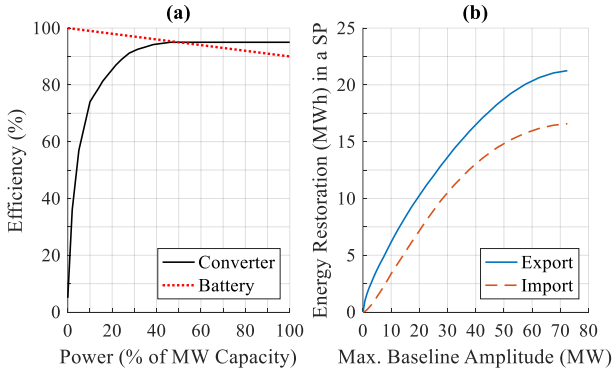

Fig. 3. (a) The efficiency curves of Li-Ion batteries and converters and (b) the resulting energy restoration (MWh) in a SP via exporting or importing baselines with different maximum amplitudes.

B. Operational Baseline Estimation

A DC provider needs to submit its operational baseline for a particular future SP at the gate closure, i.e., 1 hr before that SP. The power output $P_{B,i,t}^{op}$ and resulting SoE E_i^t of the BESS that follows the baseline $P_{B,i,t}^{BL}$ while delivering DC by $P_{B,i,t}^{DC}$ at the t^{th} time step ($t = 1, \dots, T$) within the i^{th} SP are:

$$P_{B,i,t}^{op} = P_{B,i,t}^{DC} + P_{B,i,t}^{BL} \tag{1}$$

$$E_i^t = E_i^{t-1} - P_{B,i,t}^{op} \cdot \eta_C \cdot \eta_B \cdot \Delta t \tag{2}$$

where Δt is the time step length in the simulation; terms η_C and η_B are the importing efficiencies or the reciprocal of exporting efficiencies of the converter and batteries respectively (see Fig. 3(a)), depending on the direction of the associated power flow. Driven by the SoE Rules that require a BESS provider starting a contracted EFA block with its energy footroom or headroom fulfilling the MER for the LF or HF DC delivery respectively, the operating strategy designed here specifies the target levels of initial energy footroom E_{ft} and headroom E_{hd} (MWh) that are expected to be achieved at the start of an EFA block. Then the baselines will be estimated to restore the energy that enables the BESS to meet the target levels of E_{ft} and E_{hd} prior to the subsequent EFA block. Since the baselines submitted in the i^{th} SP will take effect in the $(i+3)^{th}$ SP, the SoE level E_{i+2}^T at the end of the $(i+2)^{th}$ SP is first predicted by (3) based on the present SoE E_i^t level in combination with the baselines $P_{B,i,t}^{BL}$, $P_{B,i+1,t}^{BL}$ and $P_{B,i+2,t}^{BL}$ that have been submitted for the i^{th}, $(i+1)^{th}$ and $(i+2)^{th}$ SPs:

$$E_i^T = \max\left(\overline{E}_B,\ \min\left(\sigma \cdot \overline{E}_B,\ E_i^t - \sum_{j=t+1}^{T} P_{B,i,j}^{BL} \cdot \eta_C \cdot \eta_B \cdot \Delta t\right)\right) \tag{3a}$$

$$E_{i+1}^T = \max\left(\overline{E}_B,\ \min\left(\sigma \cdot \overline{E}_B,\ E_i^T - \sum_{j=1}^{T} P_{B,i+1,j}^{BL} \cdot \eta_C \cdot \eta_B \cdot \Delta t\right)\right) \tag{3b}$$

$$E_{i+2}^T = \max\left(\overline{E}_B,\ \min\left(\sigma \cdot \overline{E}_B,\ E_{i+1}^T - \sum_{j=1}^{T} P_{B,i+2,j}^{BL} \cdot \eta_C \cdot \eta_B \cdot \Delta t\right)\right) \tag{3c}$$

where $(T-t)$ is the number of the remaining time steps in the present i^{th} SP. The term $\overline{E}_B$ is the remaining energy capacity of the BESS and daily updated based on the SoC time series in a day through a detailed degradation model [31] which simulates the degradation $f_b(\cdot)$ of Li-Ion batteries over an elapsed time period t_E of 24 hours by combining their calendar ageing $f_t(\cdot)$ with cycle ageing $f_c(\cdot)$:

$$f_b(\cdot) = f_t\left(t_E, \widetilde{soc}, \tilde{T}_c\right) + \sum_{k=1}^{N_c} f_c\left(dod_k, soc_k, T_{c,k}\right) \tag{4}$$

where dod_k, soc_k, and $T_{c,k}$ are the depth of discharge (DoD), average SoC, and average cell temperature respectively of the k^{th} cycle ($k = 1, \dots, N_c$) which is captured from the SoC time series by using the rainflow counting algorithm [32]; and the averages of soc_k and $T_{c,k}$ within t_E are denoted by $\widetilde{soc}$ and $\tilde{T}_c$ respectively. In specific, $f_t(\cdot)$ reflects the stress of elapsed time and average stresses of SoC and cell temperature, while $f_c(\cdot)$ simulates the stresses of DoD, SoC and cell temperature of each cycle. These are formulated by (5) and (6).

$$f_t(\cdot) = S_t(t_E) \cdot S_s(\widetilde{soc}) \cdot S_T\left(\tilde{T}_c\right) \tag{5}$$

$$f_c(\cdot) = c_k \cdot S_d(dod_k) \cdot S_s(soc_k) \cdot S_T\left(T_{c,k}\right) \tag{6}$$

where the term c_k equals 0.5 or 1 when the k^{th} cycle is a half or full cycle; and the stress models $S_t(\cdot)$, $S_s(\cdot)$, $S_T(\cdot)$ and $S_d(\cdot)$ for elapsed time, SoC, cell temperature and DoD are formulated by (7)-(10) respectively.

$$S_t(t_E) = \gamma_E \cdot t_E \tag{7}$$

$$S_s(soc) = \exp\left(\gamma_s \cdot (soc - soc^{ref})\right) \tag{8}$$

$$S_T(T_c) = \exp\left(\gamma_T \cdot \left(T_c - T_c^{ref}\right) \cdot \left(T_c^{ref}/T_c\right)\right) \tag{9}$$

$$S_d(dod) = (\gamma_{d1} \cdot dod^{\gamma_{d2}} + \gamma_{d3})^{-1} \tag{10}$$

where terms γ_E, γ_s, γ_T, γ_{d1}, γ_{d2} and γ_{d3} are the coefficients of the associated stress models; and terms soc^{ref} and T_c^{ref} are the reference SoC and the reference cell temperature equalling 50% and 25℃ respectively. Based on the degradation estimated for each day d, denoted by $f_{b,d}$ ($d = 1, \dots$), the remaining energy capacity $\overline{E}_B$ of the BESS is calculated by:

$$\overline{E}_B = E_B^R \cdot \left(\lambda_{SEI} \cdot \exp\left(-\beta_{SEI} \cdot \sum_d f_{b,d}\right) + (1 - \lambda_{SEI}) \cdot \exp\left(-\sum_d f_{b,d}\right)\right) \tag{11}$$

where E_B^R is the energy capacity (MWh) of the BESS; and λ_{SEI} is the portion of the normalised energy capacity associated with the solid electrolyte interphase (SEI) film which is presumed to fade at a rate equalling the product of $f_{b,d}$ and a coefficient β_{SEI}, while the rest portion $(1 - \lambda_{SEI})$ fades at a rate of $f_{b,d}$. Table I tabulates the values of the stress model parameters adopted here which were tuned based on the lithium manganese oxide (LMO) battery degradation test data [31].

TABLE I
STRESS MODEL PARAMETERS FOR LMO BATTERY DEGRADATION

Parameter	Value	Parameter	Value
γ_E	4.14×10^{-10} (sec^{-1})	γ_{d1}	1.40×10^{5}
γ_s	1.04	γ_{d2}	-5.01×10^{-1}
γ_T	6.93×10^{-2}	γ_{d3}	-1.23×10^{5}
λ_{SEI}	5.75×10^{-2}	β_{SEI}	121

The degradation model excels in describing the capacity loss of the BESS operating at medium and high SoC levels, though it will underestimate the degradation for the operation at low SoC levels [31]. Therefore, a minimum SoC limit σ equalling 20% [33] is specified in this work to avoid excessively low SoC levels which would otherwise increase the battery impedance

and accelerate the cycle ageing [31]. Given the SoE prediction E_{i+2}^{T} in (3), the total energy E_{i+2}^{gap} required to import (-ve) or export (+ve) for restoring to E_{ft} or E_{hd} before the subsequent EFA block is estimated by:

$$E_{i+2}^{gap} = \begin{cases} E_{i+2}^{T} - \left(E_{ft} + \sigma \cdot \overline{E}_B\right), \forall\, E_{i+2}^{T} < \left(E_{ft} + \sigma \cdot \overline{E}_B\right) \\ 0, \quad \forall \left(E_{ft} + \sigma \cdot \overline{E}_B\right) \le E_{i+2}^{T} \le \left(\overline{E}_B - E_{hd}\right) \\ E_{i+2}^{T} - \left(\overline{E}_B - E_{hd}\right), \quad \forall\, E_{i+2}^{T} > \left(\overline{E}_B - E_{hd}\right) \end{cases} \quad (12)$$

Finally, when it comes to the end of the i^{th} SP (i.e., $t = T$, the Gate Closure of the $(i+3)^{th}$ SP), the maximum amplitude and associated shape of the baselines $P_{B,i+3,t}^{BL}$ $(t = 1, \dots, T)$ are submitted for the $(i+3)^{th}$ SP. They are determined to recover or release the energy quantified by the median of (a) E_{i+2}^{gap}, (b) the average energy $\left(E_{i+2}^{gap}/N\right)$ distributed across N SPs from the $(i+3)^{th}$ SP to the start of its subsequent EFA block, and (c) 20% of the MER as required by the SoE Rules, subject to the ramping limits and the rise of the BESS power capacity P_B^R above P_{DC}^{HF} or P_{DC}^{LF}. This not only fulfils the SoE restoration requirement in the SoE Rules but can also reduce the maximum amplitude of the baselines, avoiding an excessive rise of P_B^R above P_{DC}^{HF} or P_{DC}^{LF} that is required to enable full responses while respecting the baselines.

It is noted that the prediction of E_{i+2}^{T} in (3) does not consider the varying DC responses that might occur until the end of the $(i+3)^{th}$ SP due to the low predictability of grid frequencies. The unforeseen DC events may result in the BESS not meeting E_{ft} or E_{hd} at the start of the subsequent EFA block. To deal with the uncertainty of initial energy footroom and/or headroom, the rise(s) of E_{ft} and/or E_{hd} above the MER will be optimised to ensure the BESS meeting the MER of the SoE Rules for the majority of EFA blocks while avoiding the use of excessive E_{ft} or E_{hd} which would otherwise oversize the BESS in E_B^R.

C. Coordination between WF and BESS

1) Non-power-exchange (NPE) system configuration

One of the two particular WF and BESS co-location system configurations explored here is a non-power-exchange (NPE) configuration, as shown in Fig. 4 where a BESS with power and energy capacities of P_B^R and E_B^R is co-located with a WF for the DC provision and does not interchange energy with the WF.

Due to the low predictability of frequency deviations in the 1-hr period before the SP where the operational baseline takes effect, the BESS delivering the LF (or HF) service on the basis of the baseline might run towards $\sigma \cdot \overline{E}_B$ (or $\overline{E}_B$). Therefore, the BESS power output $P_{B,i,t}^{op} = \left(P_{B,i,t}^{DC} + P_{B,i,t}^{BL}\right)$ being constrained by (13) may result in the under-delivery of the LF (or HF) DC given an insufficient footroom (or headroom) in the BESS.

$$\left|P_{B,i,t}^{op} \cdot \eta_C \cdot \eta_B\right| \cdot \Delta t \le \begin{cases} E_i^{t-1} - \sigma \cdot \overline{E}_B, & \forall P_{B,i,t}^{op} > 0 \\ \overline{E}_B - E_i^{t-1}, & \forall P_{B,i,t}^{op} < 0 \end{cases} \quad (13)$$

Due to the limited ampacity of the common connection point, the co-located BESS exporting to the main grid (i.e., $P_{B,i,t}^{op} > 0$) will compress the headroom in connection ampacity available for the WF, which may cause wind curtailment especially over high wind periods. In this study, the power flow across WF meter is assumed to be limited by the connection ampacity only. To avoid any of the HF response (i.e., $P_{B,i,t}^{DC} < 0$) or the baseline for energy recovery (i.e., $P_{B,i,t}^{BL} < 0$) unexpectedly coming from the exceedance of available wind power $P_{WF,i,t}^{tot}$ over the connection ampacity P_C, i.e., the wind power to be curtailed, the power flow across WF meter $P_{WF,i,t}^{sell}$ is additionally constrained by P_C in this work. This is formulated by (14).

$$P_{WF,i,t}^{sell} = \min\left(P_{WF,i,t}^{tot},\ \left(P_C - P_{B,i,t}^{op}\right),\ P_C\right) \quad (14)$$

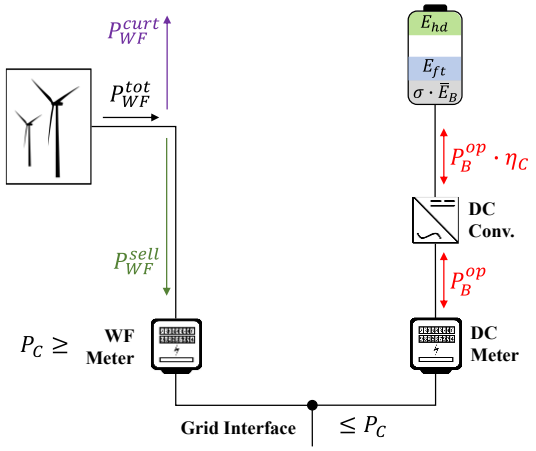

Fig. 4. The NPE configuration for the WF and BESS co-location system.

2) Power-exchange (PE) system configuration

Fig. 5 shows the second co-location configuration that places an additional converter (AdC) with power capacity of $P_A^R \le P_B^R$ behind the meters in order to permit the BESS storing otherwise curtailed wind generation for free energy recovery and/or discharge excess energy to WF meter for the wind generation benefit associated with imbalance prices. The efficiency η_A of the AdC is assumed to follow the same curve in Fig. 3(a).

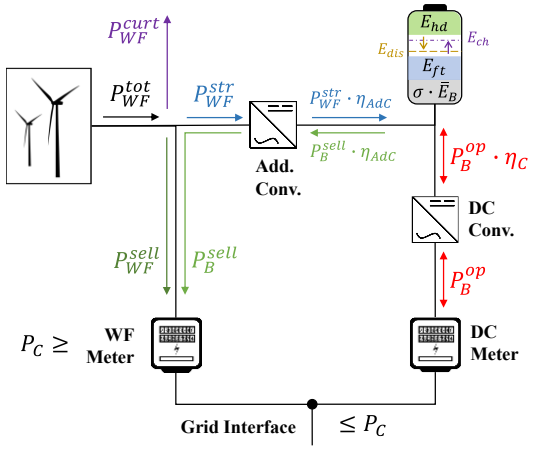

Fig. 5. The PE configuration for the WF and BESS co-location system.

The power flow across DC meter $P_{B,i,t}^{op}$ and the WF export across WF meter $P_{WF,i,t}^{sell}$ are first determined by (13) and (14)

respectively in the same way as the NPE configuration. Then two additional variables, i.e., α_{ch} and α_{dis} within [0,1], are introduced into the operating strategy to define a pair of SoE levels denoted by E_{ch} and E_{dis} (see Fig. 5) which are used to guide the time shift of wind generation via the AdC:

$$E_{ch} = \left(\sigma \cdot \overline{E}_B + E_{ft}\right) + \alpha_{ch} \cdot \left(\overline{E}_B - \sigma \cdot \overline{E}_B - E_{ft} - E_{hd}\right) \quad (15)$$

$$E_{dis} = \left(\sigma \cdot \overline{E}_B + E_{ft}\right) + \alpha_{dis} \cdot \left(\overline{E}_B - \sigma \cdot \overline{E}_B - E_{ft} - E_{hd}\right) \quad (16)$$

If E_{i+2}^T at the end of the $(i+2)^{th}$ SP is forecast to be smaller than E_{ch}, the BESS will absorb the otherwise curtailed wind power $P_{WF,i,t}^{str}$ subject to $(E_{ch} - E_{i+2}^T)$ and the available power capacities of the AdC and the BESS that is delivering $P_{B,i,t}^{op}$. For E_{i+2}^T exceeding E_{dis}, the BESS will discharge the excess energy to WF meter via the AdC. To avoid any flow to the main grid via WF meter unexpectedly coming from HF responses (which should be imported by the BESS), the export from the BESS via WF meter $P_{B,i,t}^{sell}$ is limited to zero in HF events. In deadband or LF events (i.e., $P_{B,i,t}^{DC} \geq 0$), $P_{B,i,t}^{sell}$ is calculated based on $(E_{i+2}^T - E_{dis})$ subject to the remaining ampacity across WF meter $(P_C - P_{WF,i,t}^{sell})$ and across connection point $(P_C - P_{WF,i,t}^{sell} - P_{B,i,t}^{op})$ as well as the available power capacities of the AdC and the BESS that is delivering $P_{B,i,t}^{op}$. The optimisation of α_{ch} and α_{dis} will help find the possible SoE regions suitable for the designed interaction between WF and BESS. Given the additional BESS import $P_{WF,i,t}^{str}$ or export $P_{B,i,t}^{sell}$ via the AdC, the SoE $E_i^{t\prime}$ of the BESS is updated by:

$$E_i^t = E_i^{t-1} - \left(P_{B,i,t}^{op} \cdot \eta_C + \left(P_{WF,i,t}^{str} + P_{B,i,t}^{sell}\right) \cdot \eta_A\right) \cdot \eta_B \cdot \Delta t \quad (17)$$

III. Techno-Economic Optimisation by PSO Algorithm

A. DC Availability Payment

The LF or HF DC payment for the e^{th} EFA block, denoted by R_e^{LF} or R_e^{HF} respectively, is estimated here by comparing the initial energy footroom or headroom with the MER:

$$R_e^{LF} = \mathcal{P}_{DC}^{LF} \cdot P_{DC}^{LF} \cdot 4\text{hr} \cdot \mathbb{I}\left(\left(E_{i=1}^{t=0} - \sigma \cdot \overline{E}_B\right) \geq \frac{P_{DC}^{LF} \cdot \eta_C \cdot \eta_B}{4/\text{hr}}\right) \quad (18)$$

$$R_e^{HF} = \mathcal{P}_{DC}^{HF} \cdot P_{DC}^{HF} \cdot 4\text{hr} \cdot \mathbb{I}\left(\left(\overline{E}_B - E_{i=1}^{t=0}\right) \geq \left|\frac{-P_{DC}^{HF} \cdot \eta_C \cdot \eta_B}{4/\text{hr}}\right|\right) \quad (19)$$

where $E_{i=1}^{t=0}$ denotes the initial SoE level at the start of the block. The operator $\mathbb{I}(\cdot)$ equals one if the initial footroom $\left(E_{i=1}^{t=0} - \sigma \cdot \overline{E}_B\right)$ or headroom $\left(\overline{E}_B - E_{i=1}^{t=0}\right)$ is greater than or equal to the MER, and zero otherwise. The average price of the LF DC was reported to be around £17/MW/h during the soft launch [28]. This is higher than the prevailing market prices of other FR products and is likely to decrease with the DC market growth. To perform a reasonable evaluation on the DC revenue under stable DC markets in the future, the LF and HF DC prices (i.e., $\mathcal{P}_{DC}^{LF}$ and $\mathcal{P}_{DC}^{HF}$) are assumed here to be £8/MW/h which is close to the average DLH price [18]. It is noted that a BESS is generally used to provide both LF and HF DC as a joint service, in which case it will receive a single DC payment based on the contracted capacity P_{DC} and price $\mathcal{P}_{DC}$ rather than separate LF and HF DC payments. This is formulated by:

$$R_e^{DC} = \mathcal{P}_{DC} \cdot P_{DC} \cdot 4\text{hr} \cdot \mathbb{I}\left(\left(E_{i=1}^{t=0} - \sigma \cdot \overline{E}_B\right) \geq \frac{P_{DC} \cdot \eta_C \cdot \eta_B}{4/\text{hr}}\right) \cdot \mathbb{I}\left(\left(\overline{E}_B - E_{e,i=1}^{t=0}\right) \geq \left|\frac{-P_{DC} \cdot \eta_C \cdot \eta_B}{4/\text{hr}}\right|\right) \quad (20)$$

B. Economics related to Operational Baseline

The co-location system will need to contract with suppliers (or generators) in the electricity market for the baseline to be followed by the BESS for its energy release (or recovery) in a SP. Though these contracts would be made within the day, the day-ahead electricity prices in the UK [34] are employed here to approximate the private contract prices $\mathcal{P}_{e,i}^{BL}$ (£/MWh) and estimate the associated benefits (or costs) R_e^{BL} in the e^{th} block:

$$R_e^{BL} = \sum_i \sum_t \mathcal{P}_{e,i}^{BL} \cdot P_{B,e,i,t}^{BL} \cdot \Delta t \quad (21)$$

C. Green Subsidy

The co-location of the BESS with the WF for the DC delivery will affect the wind export to the main grid and associated green subsidies when compared to a single WF whose export to the main grid is assumed here to be the minimum of P_{WF}^{tot} or P_C. The Contracts for Difference [35] is the UK's main green subsidy scheme. It pays an accredited renewable generator for exporting to the main grid at a unit price $\mathcal{P}_{CFD}$ (£/MWh) which equals the deviation of a technology-based strike price from an electricity market reference price. Based on the averages of the strike and reference prices assigned to offshore wind over 2017-2019 [36], i.e., £165.8/MWh and £48.7/MWh respectively, the price $\mathcal{P}_{CFD}$ is approximated here to be £117.1/MWh and used to calculate the green subsidy variation δR_e^{CFD} due to the BESS co-location in the e^{th} EFA block:

$$\delta R_e^{CFD} = \sum_i \sum_t \mathcal{P}_{CFD} \cdot \left(P_{WF,i,t}^{sell} - \min\left(P_{WF,i,t}^{tot}, P_C\right)\right) \cdot \Delta t \quad (22)$$

D. Energy Imbalance Charge (EIC)

If the actual wind export to the main grid does not match the contracted volume in a SP, the WF will pay (or be paid) for its net deficit (or surplus) of energy imbalance at an imbalance price $\mathcal{P}_{e,i}^{EIC}$ (£/MWh) that reflects the expenses of the NGESO balancing transmission systems in that SP [37]. Therefore, the difference in the energy flow across WF meter between the co-location system and a single WF will determine the WF's EIC change in a SP. According to [13], DC responses will also incur in EICs. Compared to a single WF, the total EIC change δR_e^{EIC} after the BESS co-location in the e^{th} block is calculated by:

$$\delta R_e^{EIC} = \sum_i \sum_t \mathcal{P}_{e,i}^{EIC} \cdot \left(\left(P_{WF,i,t}^{sell} + P_{B,i,t}^{sell} - \min\left(P_{WF,i,t}^{tot}, P_C\right)\right) + \left(P_{B,i,t}^{op} - P_{B,i,t}^{BL}\right)\right) \cdot \Delta t \quad (23)$$

E. BESS and Connection Costs

The capital expenditure (CAPEX) C_{CAPEX} of a Li-Ion BESS is mainly attributed to the batteries, converters and balance-of-systems [38]. The unit price of Li-Ion batteries is extracted from their price trends modelled based on high-profile reports in [39], approximately equalling £128k/MWh in 2020. The prices of the converters for a utility-scale BESS and balance-of-systems are assumed here to be around £66k/MW and 30% of the overall investments into batteries and converters, respectively [38]. The annual operational expense (OPEX) C_{ann}^{OPEX} of the BESS is assumed to be 2% of its CAPEX [38]. Co-locating a BESS to an existing transmission-level WF in the UK will incur in an application fee C_{APPL} and affect balancing services (BS) and transmission network (TN) use of system (UoS) charges. Given an existing connection point between 100 MW and 1320 MW, the one-off C_{APPL} without varying the transmission entry capacity is around £105.2k based on the median base cost of six connection zones [40]. By using the BSUoS price $\mathcal{P}_{e,i}^{BS}$ (£/MWh) assigned to each SP [41], the BSUoS cost variation δC_e^{BS} in the e^{th} block after the BESS co-location is estimated from the difference in the net energy flow across the connection point:

$$\delta C_e^{BS} = \sum_i \sum_t \mathcal{P}_{e,i}^{BS} \cdot \left(\left|P_{WF,i,t}^{sell} + P_{B,i,t}^{sell} + P_{B,i,t}^{op}\right| - \min\left(P_{WF,i,t}^{tot}, P_C\right)\right) \cdot \Delta t \quad (24)$$

The TNUoS charges paid by the co-location system explored here depend on its predominant fuel type, i.e., the intermittent, in which case the annual TNUoS charge growth δC_{ann}^{TN} due to the BESS operation is determined by the growth of annual load factor (ALF) of the system [42]. Given that an ALF estimate of 10.8% would be used for a BESS prior to any historic data being available, the ALF of the co-location system is assumed to rise by 10.8%× P_B^R/P_C, leading to δC_{ann}^{TN} =£919.6/MW× P_B^R based on the tariffs specified for a particular zone in 2019/20 [43].

F. Particle Swarm Optimisation (PSO)

Given the need of derivative-free, multivariate optimsiation and the complexity in the techno-economic simulation of the co-location system, the PSO algorithm [44] is used here as an optimisation tool to determine the best BESS capacity and strategy variables that maximise the NPV of the co-location system in the NPE or PE configuration. For each generated particle which represents a vector of optimisation variables, the power and energy flows of the system are simulated until $\overline{E}_B$ falls below the retention limit of 80% or cannot support E_{ft} and/or E_{hd}. Since most of the monetary items are monthly billed in this case, present values of the monthly cash flows are discounted by an annual return of 8% to calculate the NPV of the co-location project:

$$NPV = -C_{CAPEX} - C_{APPL} + \sum_{m=1}^{M} \frac{\sum_e \left(R_{m,e}^{DC} + R_{m,e}^{BL} + \delta R_{m,e}^{CFD} + \delta R_{m,e}^{EIC} - \delta C_{m,e}^{BS}\right) - \delta C_m^{TN} - C_m^{OPEX}}{(1+8\%)^{m/12}} \quad (25)$$

where m is a month index starting from 1 to the BESS lifetime of M months, and C_m^{OPEX} or δC_m^{TN} is the monthly BESS OPEX or TNUoS charge increase equalling $C_{ann}^{OPEX}/12$ or $\delta C_{ann}^{TN}/12$ respectively. In the optimisation, the NPV of the co-location system providing the LF or HF DC only or their joint service is maximised subject to the following technical requirements:

$$x_{LF} \cdot 1 \le P_{DC}^{LF} \le x_{LF} \cdot \min(P_B^R \cdot \eta_C, 100) \quad (26a)$$

$$x_{HF} \cdot 1 \le P_{DC}^{HF} \le x_{HF} \cdot \min(|-P_B^R|, 100) \quad (26b)$$

$$\frac{\left(x_{LF} \cdot P_{DC}^{LF} \cdot \eta_C \cdot \eta_B + x_{HF} \cdot |-P_{DC}^{HF} \cdot \eta_C \cdot \eta_B|\right)}{4/\mathrm{hr}} \le (1-\sigma) \cdot E_B^R \quad (27a)$$

$$x_{LF} \cdot E_{ft} + x_{HF} \cdot E_{hd} \le (1-\sigma) \cdot E_B^R \quad (27b)$$

$$\sum_{t=1}^{T} \left|P_{B,i,t}^{BL} \cdot \eta_C \cdot \eta_B\right| \cdot \Delta t \ge 20\% \cdot \frac{P_{DC}^{LF} \cdot \eta_C \cdot \eta_B}{4/\mathrm{hr}} \quad \text{for } \max\left(-P_{B,i,t}^{BL}\right) = \min(P_B^R - P_{DC}^{HF}, 72.5\% \cdot P_{DC}^{LF}) \quad (28a)$$

$$\sum_{t=1}^{T} P_{B,i,t}^{BL} \cdot \eta_C \cdot \eta_B \cdot \Delta t \ge 20\% \cdot \left|\frac{-P_{DC}^{HF} \cdot \eta_C \cdot \eta_B}{4/\mathrm{hr}}\right| \quad \text{for } \max\left(P_{B,i,t}^{BL}\right) = \min(P_B^R \cdot \eta_C - P_{DC}^{LF}, 72.5\% \cdot P_{DC}^{HF}) \quad (28b)$$

where the dummy variable x_{LF} or x_{HF} is set to one if the LF or HF DC is provided, and zero otherwise. Eq. (26) specifies the 100 MW unit cap on the DC contracted capacity. Furthermore, the available SoE range of the BESS above the minimum SoC limit σ must be greater than or equal to the MER and the target energy footroom/headroom, as formulated by (27a) and (27b) respectively. The requirement on the capability of restoring at least 20% of the MER via importing or exporting baselines in a SP is formulated by (28a) or (28b) where the maximum baseline amplitude is subjected to the ramp rate limits and the rise of the charging or discharging power capacity of the BESS above P_{DC}^{HF} or P_{DC}^{LF}, respectively.

It is noted that even though the PSO algorithm has the main advantages of being less sensitive to the nature of the objective function and having fewer parameters to adjust in comparison with other heuristic optimisation algorithms [45], an ordinary PSO algorithm may be trapped at a premature or local optimum solution especially to a high-dimensional problem [46]. In order to minimise the risk of falling in premature solutions, a large number of randomly initialised particles were generated by the PSO algorithm which converged to the same solution between different runs in this work. Though this suggests that the global optimum solution could have been identified in the search space, an advanced global PSO algorithm [46] could be applied to the BESS optimisation to increase the efficiency and reliability of finding the global minima.

IV. Optimisation and Simulation Results

The techno-economic simulation of the co-location system and the implementation of the PSO algorithm are accomplished in MATLAB/Simulink [47]. The BESS optimisation method is tested in the context of a particular 432 MW WF in the UK with an estimated P_C of 389 MW (i.e., 90% of the installed capacity [48]). The available power outputs of the WF over 2016-2019

are estimated from the hourly MERRA-2 wind reanalysis data [49] through a virtual wind farm model developed in [50] which takes into account the wind power smoothing effect. The GB's grid frequency [51], $\mathcal{P}_{e,i}^{BL}$ [34], $\mathcal{P}_{e,i}^{EIC}$ [52], and $\mathcal{P}_{e,i}^{BS}$ [41] in the same period are employed to compute the DC response required, baseline-related economics, EIC, and BSUoS costs respectively. It is noted that this paper focusing on the BESS optimisation at the planning stage of a co-location project relies on the multi-year techno-economic simulation without including short-term uncertainties of wind power predictions, though the bidding and operating strategies of a deployed BESS can be adjusted in the short term based on probabilistic wind power predictions across an upcoming 4-hr EFA block or more blocks.

This section first discusses the optimisation results of the co-location system for LF-only, HF-only or LF+HF DC provision, followed by presenting the service performance and the system operation under each configuration. Then the profitability of co-locating a BESS for DC provision will be analysed, suggesting the minimum possible DC tendered price.

A. Optimisation Results and BESS Usage

The BESS capacity and strategy variables optimised for the provision of LF and/or HF DC in the NPE or PE configuration are listed in Table II respectively. While the optimal contracted DC capacity reaches the 100 MW unit cap in all the scenarios, the BESS power capacity P_B^R is optimised to be around (a) 105.3 MW (i.e., 100 MW/95%) in the LF-only scenario due to the converter's export efficiency; (b) 100 MW in the HF-only scenario which just equals the HF DC (importing) capacity; and (c) 116.8 MW in the LF+HF scenario where the BESS needs excess power capacity to accommodate the baselines that are in the same direction as DC responses. Since the baseline and the DC response are always in opposite directions when either LF or HF DC is provided only, the BESS is allowed to fully use its power capacity to maximise the baseline amplitude for the SoE restoration subject to the ramp rate limit. It is estimated that the BESS can import up to 16.6 MWh or export up to 21.2 MWh through baselines over a 30-min SP in the LF-only or HF-only scenario, fully meeting the SoE restoration requirement which is 20% of the MER of 29.2 MWh for LF DC or 21.5 MWh for HF DC, respectively. In the LF+HF scenario, the maximum amplitude of the importing or exporting baseline is determined by the rise of P_B^R above P_{DC}^{HF} or the rise of $(P_B^R \cdot \eta_C)$ above P_{DC}^{LF}, equalling around 16.8 MW or 11 MW respectively. This allows the BESS to replenish 5.8 MWh or release 6.8 MWh over a SP, still meeting the required 20% of the MER (i.e., 28.9 MWh for LF DC and 21.8 MWh for HF DC).

In addition, the deployment of an AdC for behind-the-meter energy interchange between WF and BESS is not suggested by the optimsiation (i.e., $P_A^R = 0$). This is because the extra BESS cycles combined with the increased DoD would accelerate the battery degradation and thus reduce the project's lifespan and total payments from DC delivery. Fig. 6 shows the SoC changes and the resulting energy capacity fading of the 116.8 MW, 87.8 MWh BESS in the optimised NPE configuration (see Table II) or in a presumed PE configuration which adopts a 5 MW AdC with α_{dis} and α_{ch} equalling 40% and 60% respectively. The PE-based BESS with greater SoC fluctuations is shown to degrade faster and reaches the retention limit of 80% at around 10.8 years, which is half a year shorter than the 11.3-year lifetime of the NPE-based BESS. Even though the absorption of otherwise curtailed wind generation via the AdC could offer free energy for SoE recovery, the savings in the costs of negative (importing) operational baselines cannot compensate for the AdC investment and revenue losses such as DC payment reductions, which will be detailed in Section IV.C.

TABLE II-
OPTIMISATION OF CO-LOCATED BESS CAPACITY AND STRATEGY VARIABLES.

Variable	LF-only		HF-only		LF + HF	
	NPE	PE	NPE	PE	NPE	PE
P_B^R (MW)	105.3	105.3	100	100	116.8	116.8
E_B^R (MWh)	83.7	83.7	35.7	35.7	87.8	87.8
P_A^R (MW)	n/a	**0**	n/a	**0**	n/a	**0**
P_{DC}^{LF} (MW)	100	100	n/a	n/a	100	100
P_{DC}^{HF} (MW)	n/a	n/a	100	100	100	100
E_{ft} (MWh)	32.2	32.2	n/a	n/a	32.3	32.3
E_{hd} (MWh)	n/a	n/a	23.4	23.4	23.3	23.3
α_{ch}	n/a	Ineff.	n/a	Ineff.	n/a	Ineff.
α_{dis}	n/a	Ineff.	n/a	Ineff.	n/a	Ineff.
Lifetime (yrs)	11.7	11.7	15	15	11.3	11.3

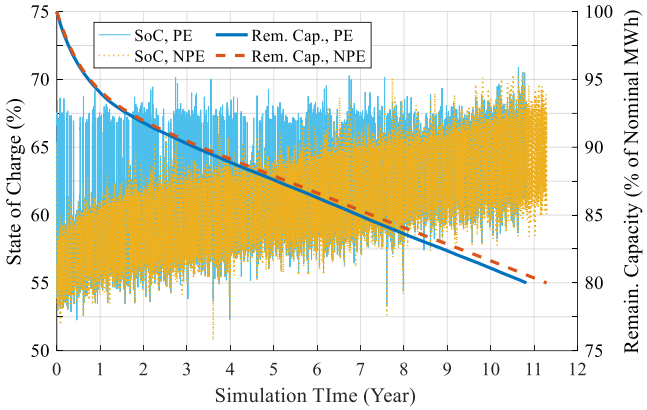

Fig. 6. The changes of SoC levels (%) and remaining energy capacity (% of the nominal capacity) of the 116.8 MW, 87.8 MWh BESS in the optimised NPE configuration or in a presumed PE configuration with a 5 MW AdC, α_{dis} = 40% and α_{ch} = 60%.

For the operating strategy, the optimum energy footroom E_{ft} or headroom E_{hd} is about 32.2 MWh or 23.4 MWh in the LF-only or HF-only scenario, which can support 16.5-min full LF responses or 16.3-min full HF responses respectively. In the LF+HF scenario, E_{ft} of 32.3 MWh and E_{hd} of 23.3 MWh allow the BESS to provide full LF and HF responses for 16.8 and 16 minutes respectively. The optimal E_{ft} and/or E_{hd} being greater than their respective MERs (i.e., 15-min full responses) indicates the need of dealing with the frequency uncertainties until the end of the 30-min baselines in question. Furthermore, when providing the DC responses that usually locate below 5% of the DC capacity, the use of a greater P_B^R will decrease the overall exporting or importing efficiency of the BESS (see Fig. 3(a)). Therefore, the 116.8 MW BESS in the LF+HF scenario requires greater E_{ft} or smaller E_{hd} (especially in terms of full-response duration) than the 105.3 MW or 100 MW BESS in the

LF-only or HF-only scenario, respectively. The SoE restoration via baselines towards the optimal E_{ft} and/or E_{hd} ensures the BESS having sufficient energy footroom and/or headroom to comply with the DC response curve all the time, as shown in Fig. 7. Even though the initial energy footroom and headroom cannot always reach the optimum E_{ft} and E_{hd} at the beginning of EFA blocks, they meet the SoE Rules by exceeding the associated MER for almost all the blocks (see Fig. 8) due to the optimised rises of E_{ft} and E_{hd} above MER. The DC responses and initial energy footroom and headroom of the BESS in the presumed PE configuration are also shown in Figs. 7(d) and 8(d). Since the SoE limits E_{dis} and E_{ch} that regulate the energy interchange of BESS and WF are specified within the region which fulfils E_{ft} and E_{hd} (see (15) and (16) in Section II.C), the PE-based BESS also performs well in delivering DC responses and meeting the MERs.

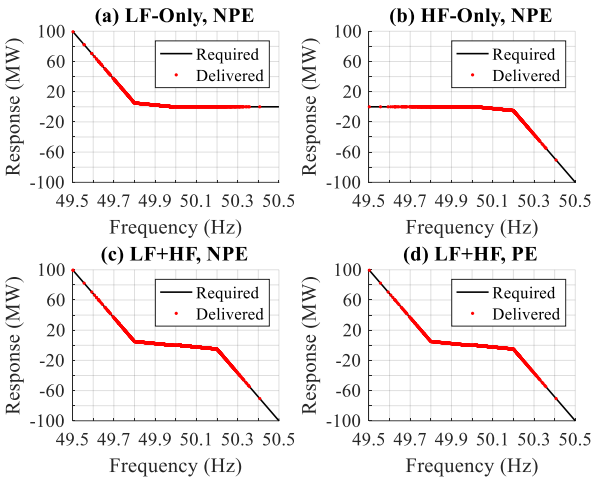

Fig. 7. DC curves against actual responses in NPE-based (a) LF-only, (b) HF-only, (c) LF+HF and (d) PE-based LF+HF scenarios.

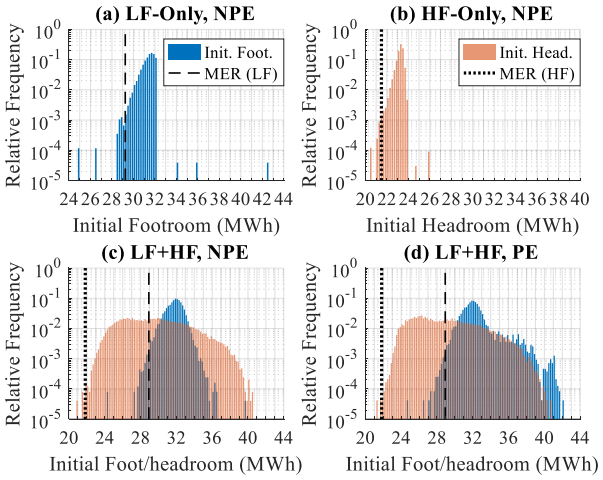

Fig. 8. Histograms of initial footroom/headroom (MWh) against MERs in NPE-based (a) LF-only, (b) HF-only, (c) LF+HF and (d) PE-based LF+HF scenarios.

The best BESS energy capacity E_B^R is around 36 MWh in the HF-only scenario and increases to around 83 – 88 MWh when the BESS provides the LF DC in LF-only and LF+HF scenarios. This is because the BESS keeping sufficient energy footroom for LF DC requires a greater E_B^R to mitigate its energy capacity degradation which would otherwise be accelerated at higher SoC levels [27]. Fig. 9 shows the SoC distributions of the BESS in different scenarios. Even though a smaller BESS is used in the HF-only scenario, its SoC levels fluctuating just above the minimum SoC limit σ reduces the degradation of the BESS which reaches the pre-defined lifespan of 15 years (see Table II). Fig. 9(d) shows the SoC distribution of the BESS in the presumed PE configuration which, compared to the SoC of the NPE-based BESS, is slightly shifted towards higher levels on average due to the additional SoE recovery from the otherwise curtailed wind generation. This also contributes to the faster degradation of the PE-based BESS due to the increased SoC stress (see (8) in Section II.B).

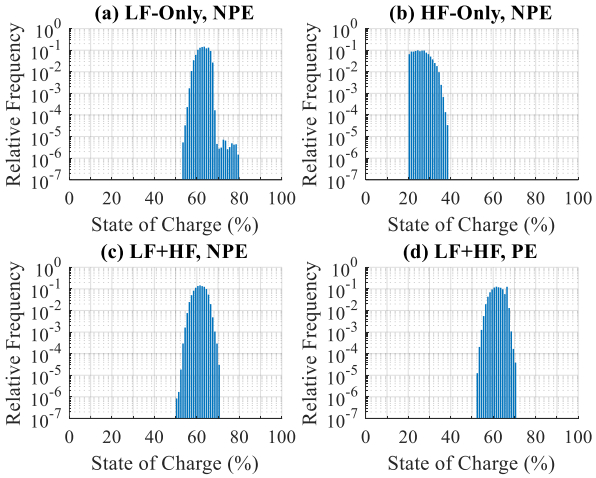

Fig. 9. Histograms of the SoC of the BESS in NPE-based (a) LF-only, (b) HF-only, (c) LF+HF and (d) PE-based LF+HF scenarios.

B. BESS Operation and Coordination with WF

1) System Operation under NPE configuration

The power outputs of WF and BESS and the resulting SoE levels simulated based on the optimised variables in the NPE-based LF+HF scenario during a particular day (commencing the 30,648th hour) are shown in Fig. 10 respectively. As was noted in Section II.B, DC responses of the BESS are the deviations of power flows across DC meter from baselines. The significant LF responses over 4 – 4.5 hr and 7 – 8.5 hr (see Fig. 10(a)) greatly reduce SoE levels, and the resulting SoE forecasts E_{i+2}^T at the end of the 1-hr-ahead SP decline below the target energy footroom stacking on the minimum SoC limit (see Fig. 10(b)). This leads to the submission of large importing baselines which take effect in the SP over 5.5 – 6 hr and 8.5 – 10 hr respectively (see 10(a)) and restore the SoE to the target footroom level (see Fig. 10(b)). The relatively greater DoD of the resulting battery cycles increases the DoD stress and thus aggravates the battery degradation (see (10) in Section II.B). In addition, given the limited ampacity of the common connection point, the WF has to curtail more export to ensure the delivery of LF responses in high wind periods, e.g., prior to 5 hr and over 7 – 8.5 hr as shown in Fig. 10(c). It is noted that even though the high wind period coincides with LF responses over 8.5 – 10 hr, the BESS

following negative baselines does not take up any export capacity of the connection point and avoids the curtailment of wind export and associated revenue losses.

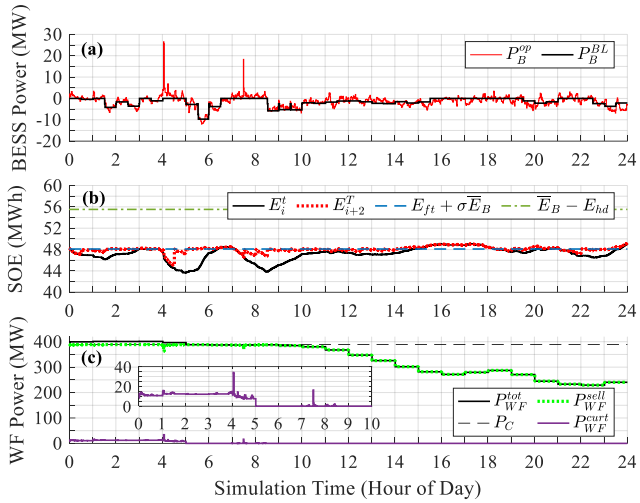

Fig. 10. (a) BESS baselines and power flows across DC meter (MW); (b) SoE (MWh) in real time and forecasts for 1-hr-ahead SPs against the levels specified by target footroom and headroom; and (c) WF power outputs and curtailment (MW) in the optimised NPE-based LF+HF scenario over a particular simulation day commencing the 30,638th hour.

2) System Operation under PE configuration

Fig. 11 shows the outputs of WF and BESS in the presumed PE-based LF+HF scenario and the resulting SoE variations over the same simulation day where the BESS starts with a SoE level close to the charging limit E_{ch}. The wind power P_{WF}^{str} which would otherwise be curtailed due to an excessive available wind output and/or LF response in the high wind period (i.e., prior to 5 hr and over 7 – 9 hr) is imported by the BESS subject to the 5 MW capacity of the AdC and the exceedance of E_{ch} over the SoE forecast E_{i+2}^{T}. The free SoE recovery by storing otherwise curtailed wind generation allows the BESS to operate above the target energy footroom stacking on the minimum SoC limit prior to 8 hr (see Fig. 11(b)), avoiding the submission and costs of the negative baselines that are required to replenish the BESS in the NPE configuration (see Figs. 10(a) and 11(a)).

However, as was noted above, the BESS export in LF events being reduced by negative baselines could alleviate the curtailment of wind export to the main grid in high wind periods. Therefore, the PE configuration mitigating the need of negative baselines could result in greater wind export curtailment than the NPE configuration. It is evaluated that the total wind export to the main grid before 8 hr is about 3,102.3 or 3,101 MWh under the NPE or PE configuration respectively, meaning the losses of green subsidies and EICs related to the wind export reductions under the PE configuration.

In addition, in the period of 6 – 7 hr where the available wind power outputs fall slightly below the connection point ampacity (see Fig. 11(c)), the rise of E_{i+2}^{T} above the discharging limit E_{dis} is exported through the AdC to WF meter subject to the ampacity headroom of the connection point (see P_B^{sell} in Fig. 11(a)). As was designed in Section II.C, all the discharge of P_B^{sell} occurs outside the HF events in order to avoid that any power flow across WF meter to the main grid unexpectedly comes from HF responses of the BESS.

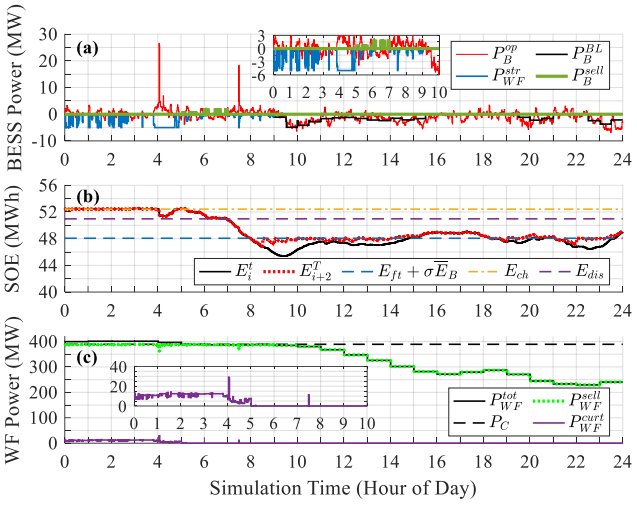

Fig. 11. (a) BESS baselines and power flows across DC meter and AdC (MW); (b) SoE (MWh) in real time and forecasts for 1-hr-ahead SPs against the levels specified by target footroom and charging/discharging limits; and (c) WF power outputs and curtailment (MW) in the presumed PE-based LF+HF scenario over a particular simulation day commencing the 30,638th hour.

C. System Profitability and Minimum DC Prices

Table III tabulates the cumulative present values of monetary components of different co-location projects simulated based on the optimised variables (or those presumed for the PE-based LF+HF scenario). Even though the co-location of the BESS increases the overall connection charges to some extent, the size-dependent BESS investments are shown to contribute the most to the total costs of the co-location projects.

Since the SoE Rules are met by the BESS for almost all the EFA blocks, the differences in DC payments between scenarios are mainly determined by the BESS lifetime. The highest DC payment is achieved in the HF-only scenario where the BESS has the longest lifetime of 15 years, while the BESS in the PE-based LF+HF scenario receives the lowest DC payment due to its greater SoC fluctuations accelerating the capacity fading and reducing the lifetime to 10.8 years (see Fig. 6). Furthermore, compared to the NPE-based LF-only scenario, the SoE recovery through HF responses in the LF+HF scenarios or the absorption of otherwise curtailed wind generation in the PE-based LF+HF scenario mitigates the need of importing baselines and reduces baseline-related costs. However, as was noted in Section IV.B, the reduced need of importing baselines which would otherwise lower the BESS export in LF events might lose the opportunity of reducing the curtailment of wind export to the main grid during high wind periods. Therefore, the BESS in the LF+HF scenario (especially in the PE configuration) is shown to cause greater reductions in green subsidies and EICs.

Given the BESS investments together with other cost growths and revenue losses being compensated by the DC payments, positive NPVs are achieved in all the scenarios tested here, indicating profitable BESS co-location projects for the DC provision. It is noted that although a relatively smaller NPV is achieved in the LF+HF scenario, linking LF DC with HF DC as

a joint service is more favourable in the DC market. In addition, the NPE-based LF+HF scenario evaluated here shows a greater NPV than the PE-based since the BESS in the PE configuration requires extra AdC investments and receives less DC payments due to a shortened lifetime.

TABLE III
THE OPTIMISATION-BASED CUMULATIVE PRESENT VALUES (£M) OF MONETARY ITEMS OF THE SYSTEMS IN NPE AND PE CONFIGURATIONS

Item	LF-only	HF-only	LF + HF	
	NPE	NPE	NPE	PE
CAPEX of BESS	–22.95	–14.51	–24.63	–25.06
OPEX of BESS	–4.24	–3.02	–4.47	–4.44
δConnection	–1.09	–1.03	–1.22	–1.15
DC Payment	53.75	62.11	52.51	51.15
δEIC (DC)	1.51	–1.83	–0.08	–0.08
Baseline-related	–4.61	0.18	–3.84	–3.15
δSubsidy (WF)	–0.18	–0.04	–0.28	–0.52
δEIC (WF)	–0.06	–0.01	–0.10	–0.17
NPV	22.13	41.85	17.90	16.59

Even though the optimisation is implemented based on half of the average price during the soft lunch of DC (i.e., £8/MW/h), the BESS co-location project still shows great potential in terms of profits. When the DC price declines to about £5.3/MW/h, it is estimated that the reduction of the overall DC payments will result in the project having a zero NPV in the LF+HF scenario. Therefore, given the particular WF and financial data adopted in this work, the minimum possible DC price for linked bids of LF DC and HF DC is expected to be at least £5.3/MW/h which could ensure the profitability of the project. It should be noted that the updated financial inputs such as DC prices will alter the trade-off between the investments into the co-location system and the revenue dominated by DC payments, which will drive the need of re-optimising the BESS size and operating strategies in new circumstances.

V. CONCLUSIONS

This paper has developed a modelling framework to optimise the capacity and operating strategies of a battery energy storage system (BESS) co-located with an existing wind farm (WF) for the delivery of frequency response (FR) services and evaluated the profitability of co-location projects under the UK FR market reforms. The operating strategies including the FR delivery and operational baseline submission for the Dynamic Containment (DC) service as well as the coordination of WF and BESS have been designed to prioritise the DC provision, followed by the wind export to the main grid. The proposed BESS optimisation method has been tested for the provision of either or both low-frequency (LF) and high-frequency (HF) DC services based on a particular 432 MW transmission-level WF in the UK.

Given a DC price of £8/MW/h, the optimisation results have indicated the profitability of a BESS co-location system which followed the specific State of Energy (SoE) Rules in almost all the contracted service windows thanks to the SoE management through operational baselines. Even though the placement of an additional converter between WF and BESS provided extra SoE management through the energy interchange behind the meters, the greater state of charge fluctuations accelerated the capacity fading and shortened the BESS lifetime for DC provision. The reductions in total DC payments together with extra converter investments make the behind-the-meter energy interchange less attractive in this work. It has been evaluated that the co-location project developed for the particular WF would be profitable if the tendered prices for linked bids of LF DC and HF DC were greater than £5.3/MW/h.

With the ongoing reforms of the UK FR service markets, the modelling framework can be developed further to simulate the other two end-state FR products and reflect the latest technical requirements and market mechanisms. Future work will also look into the optimal combination of these end-state products using as basis the process of optimisation for the contracted FR capacity and the BESS size presented in this paper.

ACKNOWLEDGMENT

This work was conducted as part of the research programme of the Electrical Infrastructure Research Hub in collaboration with the Offshore Renewable Energy Catapult.

REFERENCES

[1] Upgrading Our Energy System: Smart Systems and Flexibility Plan, Office of Gas and Electricity Markets (Ofgem), London, UK, Jul. 2017.
[2] Electricity Storage and Renewables: Costs and Markets to 2030, International Renewable Energy Agency, Abu Dhabi, UAE, Oct. 2017.
[3] Introduction to Co-location, NGESO, London, UK, Mar. 2019.
[4] F. Fan, I. Kockar, H. Xu, and J. Li, "Scheduling framework using dynamic optimal power flow for battery energy storage systems," *CESS J. Power Energy Syst.*, vol. 8, no. 1, pp. 271-280, Jan. 2022.
[5] F. Fan, G. Zorzi, D. Campos-Gaona, et al., "Sizing and coordination strategies of battery energy storage system co-located with wind farm: the UK perspective," *Energies*, vol. 14, no. 5, p. 1439, Mar. 2021.
[6] Ancillary Service Report 2017, Energy UK, London, UK, Apr. 2017.
[7] Wind Energy and On-site Energy Storage: Exploring Market Opportunities, WindEurope, Brussels, Belgium, Nov. 2017.
[8] Firm Frequency Response Tender Rules and Standard Contract Terms Issue #10, NGESO, Oct. 2019.
[9] Enhanced Frequency Response: Invitation to Tender for Pre-qualified Parties, NGESO, Jul. 2016.
[10] Response and Reserve Roadmap, NGESO, Dec. 2019.
[11] Future of Frequency Response: Industry Update, NGESO, Feb. 2019.
[12] Response Auction Trial Service Terms (Phase 2), NGESO, Nov. 2019.
[13] Dynamic Containment Service Terms (Version 4.0), NGESO, Oct. 2021.
[14] Dynamic Containment Participation Guidance Document (Version 4.0), NGESO, Sep. 2021.
[15] B. Lian, A. Sims, D. Yu, et al., "Optimizing LiFePO4 battery energy storage systems for frequency response in the UK system," *IEEE Trans. Sustainable Energy*, vol. 8, no. 1, pp. 385-394, Jan. 2017.
[16] B. Xu, Y. Shi, D.S. Kirschen, et al., "Optimal battery participation in frequency regulation markets," *IEEE Trans. Power Syst.*, vol. 33, no. 6, pp. 6715-6725, Nov. 2018.
[17] G. He, Q. Chen, C. Kang, P. Pinson, and Q. Xia, "Optimal bidding strategy of battery storage in power markets considering performance-based regulation and battery cycle life," *IEEE Trans. Smart Grid*, vol. 7, no. 5, pp. 2359-2367, Sep. 2016.
[18] F. Fan, G. Zorzi, D. Campos-Gaona, et al., "Wind-plus-battery system optimisation for frequency response: the UK perspective," *Electric Power Syst. Res.*, vol. 210, p. 108400, Oct. 2022.
[19] L. Johnston, F. Díaz-González, O. Gomis-Bellmunt, et al., "Methodology for the economic optimisation of energy storage systems for frequency support in wind power plants," *Appl. Energy*, vol. 137, pp. 660-669, Jan. 2015.
[20] S. Munoz-Vaca, C. Patsios, and P. Taylor, "Enhancing frequency response of wind farm using hybrid energy storage systems," in *Proc. 5th Int. Conf. Renewable Energy Res. Appl.*, Birmingham, UK, 2016, pp.1-5.
[21] G. He, Q. Chen, C. Kang, Q. Xia, and K. Poolla, "Cooperation of wind power and battery storage to provide frequency regulation in power

markets," in *IEEE Trans. Power Syst.*, vol. 32, no. 5, pp. 3559-3568, Sep. 2017.
[22] M. Naemi, D. Davis, and M.J. Brear, "Optimisation and analysis of battery storage integrated into a wind power plant participating in a wholesale electricity market with energy and ancillary services," *J. Cleaner Production*, vol. 373, p. 133909, Nov. 2022.
[23] J. Martinez-Rico, E. Zulueta, I.R. de Argandoña, M. Armendia, and U. Fernandez-Gamiz, "Sizing a battery energy storage system for hybrid renewable power plants based on optimal market participation under different market scenarios," *IEEE Trans. Ind. Appl.*, vol. 58, no. 5, pp. 5624-5634, Sep./Oct. 2022.
[24] F. Fan, D. Campos-Gaona, and J. Nwobu, "Wind-plus-battery system optimisation for stacking of frequency response and black start services in the UK," in *Proc. 11th Int. Conf. Power Electron. Mach. Drives*, Newcastle, UK, 2022, pp. 166-172.
[25] B. Cheng and W.B. Powell, "Co-optimizing battery storage for the frequency regulation and energy arbitrage using multi-scale dynamic programming," *IEEE Trans. Smart Grid*, vol. 9, no. 3, pp. 1997-2005, May 2018.
[26] T.A. Nguyen, R.H. Byrne, R.J. Concepcion, et al., "Maximizing revenue from electrical energy storage in MISO energy & frequency regulation markets," in *Proc. 2017 IEEE Power Energy Soc. General Meeting*, Chicago, USA, pp. 1-5.
[27] A. Mariaud, S. Acha, N. Ekins-Daukes, et al., "Integrated optimisation of photovoltaic and battery storage systems for UK commercial buildings," *Appl. Energy*, vol. 199, pp. 466-478, Aug. 2017.
[28] Dynamic Containment Soft Launch Development Document Version 2, NGESO, Jan. 2021.
[29] Dynamic Containment High (DCH) Webinar, NGESO, Sep. 2021.
[30] E. Arnieri, L. Boccia, F. Amoroso, G. Amendola, and G. Cappuccino, "Improved efficiency management strategy for battery-based energy storage systems," *Electronics*, vol. 8, no. 12, p. 1459, Dec. 2019.
[31] B. Xu, A. Oudalov, A. Ulbig, et al., "Modeling of Lithium-Ion battery degradation for cell life assessment," *IEEE Trans. Smart Grid*, vol. 9, no. 2, pp. 1131-1140, 2018.
[32] Y.L. Lee and T. Tjhung, "Chapter 3 - Rainflow cycle counting techniques," in *Metal Fatigue Analysis Handbook*, Butterworth-Heinemann: Boston, 2012, pp. 89-144.
[33] J. Jiang, W. Shi, J. Zheng, P. Zuo, J. Xiao, X. Chen, W. Xu, and J.-G. Zhang, "Optimized operating range for large-format $LiFePO_4$/Graphite batteries," *J. Electrochemical Society*, vol. 161, no. 3, pp. A336-A341, 2014.
[34] N2EX Day Ahead Auction Prices, Nord Pool. https://www.nordpoolgroup.com/Market-data1/GB/
[35] Dept. Business, Energy & Industrial Strategy, *Contracts for Difference: Policy Paper*. https://www.gov.uk/government/publications/contracts-for-difference/contract-for-difference
[36] Low Carbon Contracts Company, *Actual CfD Generation and Avoided GHG Emissions*. https://www.lowcarboncontracts.uk/data-portal/dataset/actual-cfd-generation-and-avoided-ghg-emissions
[37] The Electricity Trading Arrangements-A Beginner's Guide (Version 8.0), Elexon, London, UK, Feb. 2019.
[38] V. Jülch, "Comparison of electricity storage options using levelized cost of storage (LCOS) method," *Appl. Energy*, vol. 183, pp. 1594-1606, Dec. 2016.
[39] D. Campos-Gaona, A. Madariaga, J. Zafar, O. Anaya-Lara, and G. Burt, "Techno-economic analysis of energy storage system for wind farms: the UK perspective," in *Proc. 2018 Int. Conf. Smart Energy Syst. Technol.*, Seville, Spain, pp. 1-6.
[40] NGESO, *Application Fee Calculator 19_20_0*. https://www.nationalgrideso.com/document/154976/download
[41] NGESO, *Balancing Services Use of System (BSUoS) Charges*. https://www.nationalgrideso.com/charging/balancing-services-use-system-bsuos-charges
[42] Electricity Transmission Network Charging: An Introductory Guide, NGESO, Jan. 2018.
[43] Final TNUoS Tariffs for 2019/20, NGESO, Jan. 2019.
[44] J. Kennedy and R. Eberhart, "Particle swarm optimization," in *Proc. Int. Conf. Neural Netw.*, Perth, Australia, 1995, pp. 1942-1948.
[45] K.Y. Lee and J.-B. Park, "Application of particle swarm optimization to economic dispatch problem: advantages and disadvantages," in *Proc. 2006 IEEE PES Power Syst. Conf. Exposition*, Atlanta, GA, USA, pp. 188-192.
[46] J.J. Jamian, M.N. Abdullah, H. Mokhlis, M.W. Mustafa, and A.H.A. Bakar, "Global particle swarm optimization for high dimension numerical functions analysis," *J. Appl. Mathematics*, vol. 2014, p. 329193, Feb. 2014.
[47] MATLAB Release 2018b, The MathWorks, Inc., Mass., USA.
[48] Round 3 Offshore Wind Farm Connection Study Version 1, The Crown State, London, UK, Jan. 2009.
[49] A. Molod, L. Takacs, M. Suarez, and J. Bacmeister, "Development of the GEOS-5 atmospheric general circulation model: evolution from MERRA to MERRA2," *Geoscientific Model Development*, vol. 8, no. 5, pp. 1339-1356, May 2015.
[50] I. Staffell and S. Pfenninger, "Using bias-corrected reanalysis to simulate current and future wind power output," *Energy*, vol. 114, pp. 1224-1239, Nov. 2016.
[51] NGESO, *Historic frequency data*. https://www.nationalgrideso.com/balancing-services/frequency-response-services/historic-frequency-data
[52] Elexon, System sell & system buy prices, 2020. https://www.bmreports.com/bmrs/?q=balancing/systemsellbuyprices

Fulin Fan received the B.Eng. and Ph.D. degrees in electronic and electrical engineering from North China Electric Power University, Baoding, China, and the University of Strathclyde, Glasgow, U.K., in 2012 and 2018, respectively.

From 2016 to 2018, he was a Research Assistant with the University of Strathclyde, where he has been a Research Associate since 2018. His research interests include energy storage system optimisation, real-time thermal rating for overhead lines, HVDC cables, and transport electrification modelling.

John Nwobu has over 10 years of experience in working within the wind power, power electronics, and energy storage industry. He joined Offshore Renewable Energy Catapult in 2019 to provide input into the offshore wind electrical infrastructure research programmes. Currently he is a Senior Research Engineer in Energy Systems responsible for leading the research programme development in energy systems and maintaining an expert understanding of energy system technology innovation research areas from design to deployment, testing and full operations. He is also an author of a number of journals and conference papers.

David Campos-Gaona (Senior Member, IEEE) received the B.E. degree in electronic engineering, and the M.Sc. and Ph.D. degrees in electrical engineering, from Instituto Tecnolgico de Morelia, Morelia, Mexico, in 2004, 2007, and 2012, respectively.

From 2014 to 2016, he was a Postdoctoral Research Fellow with the Department of Electrical and Computer Engineering, University of British Columbia, Vancouver, BC, Canada. Since August 2016, he has been with the University of Strathclyde, Glasgow, U.K., first as a Research Associate and currently as a Senior Lecturer. His research interests include wind farm power integration, HVDC transmission systems, variable frequency systems, and real-time digital control of power-electronic-based devices.